LAWRENCE
LIVERMORE
NATIONAL
LABORATORY

UCRL-CONF-222465

ALE3D Simulation of Heating and Violence in a Fast Cookoff Experiment with LX-10

M. A. McClelland, J. L. Maienschein, W. M. Howard, A. L. Nichols, M. R. deHaven, O. T. Strand

June 28, 2006

13th International Detonation Symposium
Norfolk, VA, United States
July 23, 2006 through July 28, 2006

ALE3D SIMULATION OF HEATING AND VIOLENCE IN A FAST COOKOFF EXPERIMENT WITH LX-10*

Matthew A. McClelland, Jon L. Maienschein, William M. Howard,
Albert L. Nichols, Martin R. deHaven, and O. Ted Strand

Energetic Materials Center, Lawrence Livermore National Laboratory,
Livermore CA 94511

Abstract. We performed a computational and experimental analysis of fast cookoff of LX-10 (94.7% HMX, 5.3% Viton A) confined in a 2 kbar steel tube with reinforced end caps. A Scaled–Thermal-Explosion-eXperiment (STEX) was completed in which three radiant heaters were used to heat the vessel until ignition, resulting in a moderately violent explosion after 20.4 minutes. Thermocouple measurements showed tube temperatures as high as 340°C at ignition and LX-10 surface temperatures as high as 279°C, which is near the melting point of HMX. Three micro-power radar systems were used to measure mean fragment velocities of 840 m/s. Photonics Doppler Velocimeters (PDVs) showed a rapid acceleration of fragments over 80 μs. A one-dimensional ALE3D cookoff model at the vessel midplane was used to simulate the heating, thermal expansion, LX-10 decomposition composition, and closing of the gap between the HE (High Explosive) and vessel wall. Although the ALE3D simulation terminated before ignition, the model provided a good representation of heat transfer through the case and across the dynamic gap to the explosive.

INTRODUCTION

Computational tools are being developed to predict the response of munitions and propellant systems to thermal events. These simulation tools are needed to help answer questions related to fire hazards in a climate of tighter restrictions concerning safety and protection of the environment. Applications include systems with insensitive munitions, the development of sub-scale fire tests for rocket motors, the shipboard storage of munitions, fire-fighting strategies, and the development of laser weapons systems.

We have been investigating cookoff behavior using variations of the STEX system[1] shown in Figure 1. A sealed tube with heavily-reinforced ends is heated until ignition occurs. The response is characterized using thermocouples, strain gauges, PDV probes, and radar units to measure fragment velocities. The geometry of this cookoff system is relatively simple to facilitate model and code development. An effort is being made to investigate a wide range of explosives, physical processes, boundary conditions, and results for reaction violence.

We have developed ALE3D chemical, mechanical, and thermal models to predict the thermal behavior, time to explosion, and violence for slow cookoff of RDX and HMX-based explosives[2-4]. In all cases, we obtained good predictions for the time to explosion and at least satisfactory results for the thermal fields. Although

* Approved for public release, distribution is unlimited. Work performed under the auspices of the U.S. Department of Energy by University of California, Lawrence Livermore National Laboratory under contract No. W-7405-ENG-48.

some model-measurement comparisons of wall expansion were encouraging for PBXN-109 (64% RDX, 20% Al, 16% DOA/HTPB), the results showed that the accurate simulation of mechanical behavior and violence is a considerable challenge. These comparisons show that pressurization from decomposition, the closing of gaps, and the strength of the case and joints must be accurately represented to accurately predict violence.

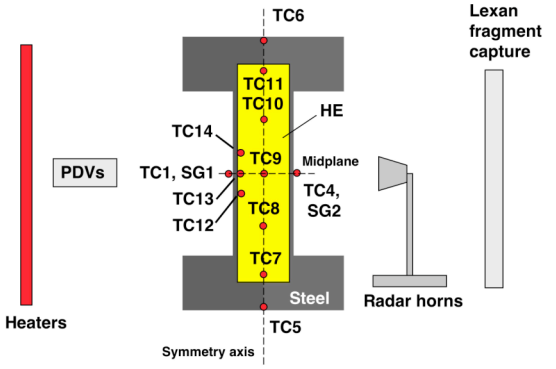

Figure 1. Schematic of geometry and instrumentation for STEX cookoff test TE-051.

In this paper, we investigate the fast cookoff of LX-10, and present STEX measurements of time to explosion, thermal behavior, and violence for LX-10 confined in an 4130 steel vessel. These measurements are compared with initial 1D predictions from an ALE3D model.

THERMAL EXPLOSION EXPERIMENT

Experimental Configuration

In order to provide violence measurements for benchmarking our ALE3D models for fast cookoff, we completed a STEX test (TE-051) for LX-10-2 confined in a 4130 steel vessel with heavily reinforced end flanges (see Figure 1). The end seals were achieved with O-rings bolted between the flange and end cap. The steel tube (5.08 cm ID X 20.32 cm L) was heat treated to give a Rockwell C hardness of 32. The wall thickness was 0.406 cm giving a confinement pressure of 200 MPa. The tube was joined to the end flange by brazing.

The LX-10 was pressed into three cylinders with a diameter of 4.93 cm, a combined length of 20.0 cm, and a density of 1.86 g/cm^3. The volumetric ullage of 7.3% was provided to allow the LX-10 to thermally expand and change from the β to δ-phase without the solid alone pressurizing the vessel cavity.

The vessel tube was heated using three 1500 W radiant heaters spaced at 120° around the vessel (see Figures 1 and 2). The normal resistance heaters for the two end caps were not employed. Radiant heater no. 1 had a 14 cm standoff from the tube axis, while the other two heaters had a standoff of 16.5 cm. We selected a smaller standoff for heater no. 1 to place the ignition point in front of this heater, approximately half way between the two end caps. In this test, these heaters were run without feedback control at maximum power. The end caps were not heated so that they would serve as heat sinks to provide a maximum temperature half way between the end caps. The radiant heaters provided an estimated maximum heat flux of 35 kW/m^2 which is in the middle of the range 5-100 kW/m^2 for cookoff in a fire.

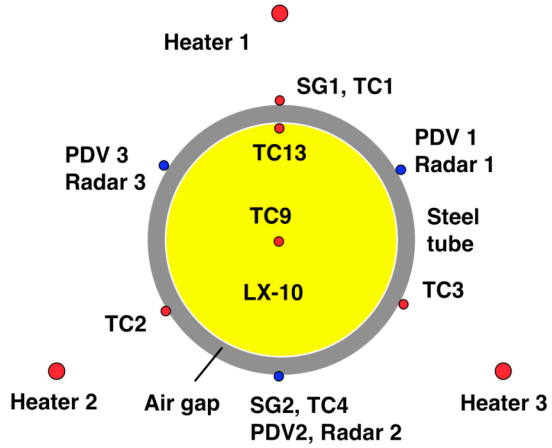

Figure 2. Instrumentation details (not to scale) at axial midplane for STEX cookoff test TE-051.

The temperature was measured at a number of locations on the vessel surface and end caps using thermocouples and Resistance Temperature Detectors (RTDs) (see Figures 1 and 2). Epoxy was used to attach the temperature sensors on the steel tube, and an additional wire strap was employed to secure TC1. It is believed that degradation was occurring to the epoxy at the highest temperatures of this test. Temperatures were measured at five positions along the HE axis using a steel probe with thermocouples and three positions near the surface of the HE. The HE surface thermocouples, consisting of 10 mil (2.54 mm) wire, were placed at a depth of 1 mm from the surface of the HE, at the angular position of heater

no.1. They were routed through small holes in an end cap and then run through the 0.75 mm gap between the vessel and the HE to the three positions on the HE surface. Epoxy was used to seal the small end cap holes and secure the thermocouples in the explosive.

Explosion violence was characterized by capturing fragments and measuring the wall position and velocity at several stages of the explosion using strain gauges, PDV probes, and micropower radar systems (see Figures 1 and 2). Two hoop (SG1, SG2) strain gauges with maximum ranges of 8 and 2%, respectively, were employed to measure the deformation of the tube near the axial midplane during the thermal ramp and subsequent explosion. These strain gauges were attached with epoxy. Three PDV probes, spaced at 120°, were used to measure the wall motion of the tube at the axial midplane over a 2 msec period during the explosion. Three radar systems were used to measure the velocity of fragments near these same locations. The rapid sampling of the strain gauges, PDV probes, and radar signals was triggered by break wires running the length of the vessel at the outside radius of the flanges. In order to capture data prior to the wire break, the data was looped through the oscilloscopes. Finally, fragments were captured in Lexan panels located on the four sides and ceiling of the shrapnel catcher.

Experimental Results for Temperature

Full power was applied in a near step function to the three radiant heaters and the explosion occurred at t=1220 secs (20.4 min). Several of the temperature measurements are plotted versus time in Figure 3 for locations shown in Figures 1 and 2. The highest temperatures were observed at the midplane location TC1 facing the nearest radiant heater (no. 1). This temperature signal increased rapidly and then more slowly as thermal losses increased to the surrounding and along the tube wall to the end caps. The maximum measured value for TC1 was 335°C at 1176 seconds when this thermocouple failed. An extrapolation of this signal gives an estimate of 340°C for TC1 at ignition. It is very likely that ignition occurred at the surface of the HE in the vicinity of this thermocouple.

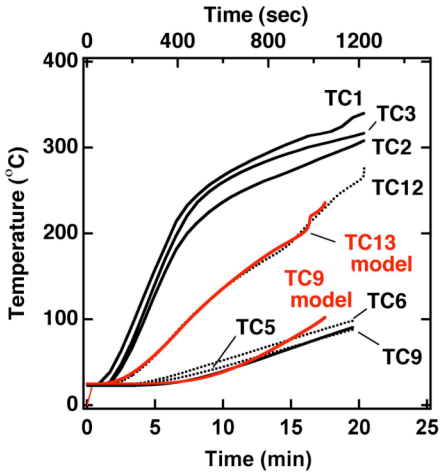

Figure 3. Measured and model temperatures vs time for STEX cookoff TE-051. The temperatures are measured unless otherwise indicated.

Note that the above estimate for the incident heat flux of 35 kW/m^2 was made based on the maximum rate of 0.6°C/sec for TC1 (see Figure 3). It was assumed that heat losses to the surroundings were negligible during this phase and the absorptivity of the steel tube was 0.26.

The midplane temperatures TC2 and TC3 facing heater nos. 2 and 3 were lower than TC1 as expected due to the larger standoffs of these heaters. Differences as large as 20°C for TC2 and TC3 indicate some asymmetry in the heating.

The lower and upper flange temperatures TC5 and TC6 increased slowly to approximately 100°C at the time of explosion. The large mass of metal (~15.2 cm D X 5.08 cm H) for each end flange assembly slowed the temperature rises relative to the much thinner tube wall. This feature kept the end cap temperatures below the tube wall temperatures, and the temperature field symmetric about the vessel midplane as desired (see Figure 1).

The five HE temperatures at the symmetry axis were all much cooler than the peak vessel temperature of 340°C (see Figures 1-3). The highest measured HE axial temperature TC9 was 93°C at the midplane at ignition (see Figure 3).

The only thermocouple at the HE surface to survive the entire heating phase was TC12 which was located 2.54 cm below the midplane (see Figures 1 and 3). TC12 increased nearly linearly from 20°C to 265°C at which point it increased

much more rapidly to 279°C at ignition. It is seen that TC11 was as much as 130°C cooler than the nearby wall temperature TC1. It is evident that the thermal transport resistance across the gap between the HE and tube was quite large. It is also observed that final temperature of 279°C is in the estimated melting point range of 275-285°C for HMX. It is possible that ignition occurred after the HMX melted, flowed, and made contact with the much hotter metal wall.

Experimental Results for Thermal Expansion

The hoop strain SG2 and the temperature TC4 are plotted versus time in Figure 4 (see Figures 1 and 2). Note that SG1, facing heater no. 1 did not provide a usable signal in this test. The curves for SG2 and TC4 have the same shape, suggesting that the tube expansion was entirely due to thermal effects prior to ignition. At the end of the heating phase the measured hoop strain SG2 was 0.3%. This is the value calculated for pure thermal expansion (CTE=12 μm/m-°C) of the steel tube at the 270°C temperature for TC4. This result suggests that there was no significant pressurization of the vessel prior to this time due to either generation of decomposition gases or contact of the LX-10 solid with the vessel wall.

Experimental results for Violence

The violence observed in STEX TE-051 was moderately high and consistent with a deflagration. The end caps and bolts were distorted, the flange sections attached to the tube were broken, but there was no flow of metal flow indicative of detonation. We recovered 203 loose fragments with a total mass comprising 45.7% of the steel tube mass between the flanges. At the time of this writing, the fragments in the Lexan panels remain to be extracted. The median fragment mass for the loose fragments was 1.1 g and a typical fragment had a dimension of scale 1 cm.

The tube wall velocity measurements from the three PDV probes and radar systems are plotted in Figure 5 versus time relative to the trigger point. The PDV measurements span four orders of magnitude. There are large oscillations visible between t=-400 and -100 μs (relative to the break wire trigger) which were likely the result of a leak-induced pressure disturbance during the ignition phase. Note that many of these measured fluctuations have a negative sign, but the PDV system cannot measure the direction of motion. A high-speed digital camera image at t=-32 μs shows bright patches near the top flange, indicating a breach of the vessel at this location. At the time of this writing additional testing has suggested possible flaws in the O-ring seals may have caused this leak.

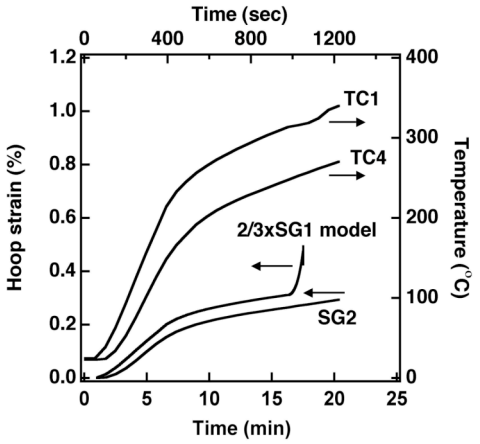

Figure 4. Measured and model temperatures and strains vs time for the heating phase of STEX fast cookoff test TE-051. The results are measurements unless otherwise indicated.

For t>-80 μs, the three PDV curves are very similar, indicating remarkable symmetry in the expansion of the tube. This symmetry occurs despite the probable surface ignition of the HE near TC1. Since this symmetry has been observed in two other cookoff experiments with LX-10[5,6] and interior ignition points, it appears that this HE-vessel system has an ability to "equilibrate" and maintain symmetry as is expands. Note that sonic transit times are of the scale 20 μs across this 5.08 cm OD LX-10 charge.

The wall velocities measured by the PDV accelerate strongly from 10 to over 1000 m/s in approximately 80 μs (see Figure 5). The three radar systems gave velocities ranging from 510 m/s for radar no. 3 to 1260 m/s for radar no. 1 with a mean of 840 m/s. Note that these velocities are themselves averages of several measurements made by each radar unit. Although the PDV measurements suggest symmetry during the explosion, the radar measurements show a much wider variation. The explosion occurs on the scale

of 80 μs, indicating a deflagration. Also, an earlier defined average[7], $v_{avg}=v_{mean}/(1+\sigma_{vel}/v_{mean})$, has a value of 580 m/s which is somewhat less than the values of 1200 and 1600 m/s for two earlier STEX tests involving the detonation of β-phase PBX-9501[7]. Here σ_{vel} is the standard deviation for the radar velocities.

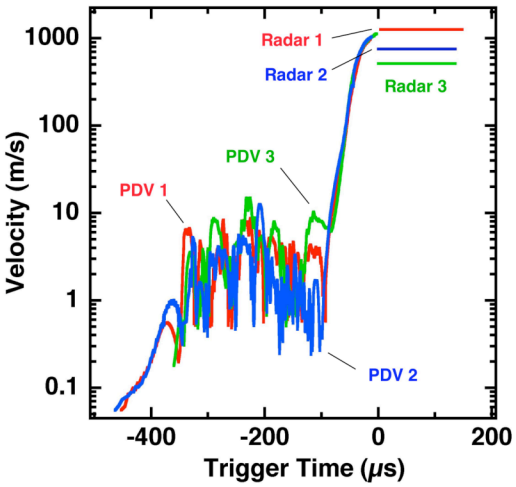

Figure 5. Tube wall velocity measurements from PDV and radar for STEX cookoff test TE-051.

Strain gauge, PDV, and radar results for the position of the tube wall and resulting fragments are plotted versus time in Figure 6. Prior to the explosive phase, beginning approximately 400 μs before the trigger wire break, the measured hoop strain SG2 was 0.3% as described above.

The position curves of Figure 6 were obtained by using the SG2 measurements until t=-60 μs. They were judged to be preferable to the PDV measurements, which do not account for the changes in direction of tube motion during this phase. We integrated the three PDV curves using the SG2 results at t=-60 μs and approximately 2% strain as the starting point. The PDV curves were extended using the associated radar velocity measurement and the final wall position calculated from the PDV integration. The linear expansion of the tube wall relative to the room temperature position is plotted on the right scale. The results from the strain gauges SG2, three PDV probes, and three radar systems provide curves for approximately 15 cm of wall motion, corresponding to 600% expansion.

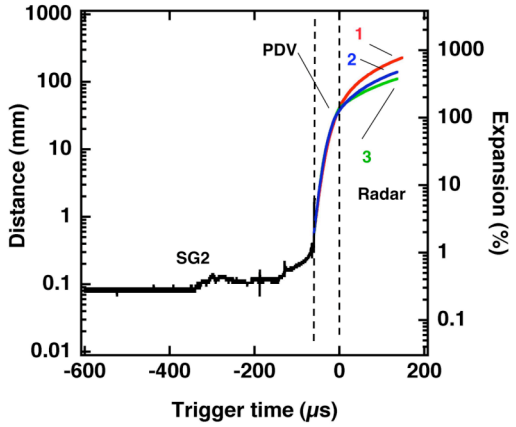

Figure 6. Tube wall position measurements from strain gauge, PDV and radar for STEX fast cookoff test TE-051.

ALE3D MODEL

Materials Models

ALE3D chemical, mechanical, and thermal models have been developed to model the cookoff of LX-10 in the STEX test (TE-051) described above. The decomposition of HMX in the LX-10 is modeled by four-step chemical kinetics based on the model reported by Tarver[8]. The first two steps are endothermic and the final two steps are exothermic.

$$A \rightarrow B \qquad r_1 = Z_1 \exp(-E_1/RT)\rho_A \qquad (1)$$

$$B \rightarrow C \qquad r_2 = Z_2 \exp(-E_2/RT)\rho_B \qquad (2)$$

$$C \rightarrow D \qquad r_3 = Z_3 \exp(-E_3/RT)\rho_C \qquad (3)$$

$$D \rightarrow E \qquad r_4 = Z_4 \exp(-E_4/RT)\rho_D^2 \qquad (4)$$

Viton is treated as an inert material during the decomposition phase, and reacts exothermically to completion during the burn phase. Here ρ_i is the mass concentration of a reactant i. The quantities r_j, Z_j, and E_j are the reaction rate, frequency factor and activation energy, respectively, for a reaction j. The components A and B are the solid species β- and δ-HMX, C is a solid intermediate, and D and E are intermediate and final gas products. The determination of the chemical kinetics parameters is described below.

After the Arrhenius reaction rates have increased to the point where changes are occurring on the time scale of sound propagation, a switch is made to a burn front model in which reactants are converted to products in a single reaction step. We assume that the burn front velocity, V, is a function of the pressure, p, at the front location, and use power-law expressions of the form to describe segments of the burn front curve:

$$V = V_0(p/p_0)^n \qquad (5)$$

Here the subscript 0 indicates a reference quantity. Although this model is part of our cookoff framework it was not used in this paper since numerical difficulties terminated our simulation prior to the switch from the decomposition model (Eqs. (1)-(4) to Eq. (5). The determination of burn rate parameters for LX-10 from high pressure strandburner measurements is discussed elsewhere[5].

The mechanical behavior of the condensed HE constituents (HMX A, HMX B, HMX C), the Viton reactant, and the steel is represented by Steinberg-Guinan mechanical models with a 7-term polynomial equation of state. The constant volume heat capacity does not vary with temperature in this EOS. Calculated melt and cold curves are used to account for the influence of compression on melting energy. A nonlinear regression procedure was used to determine the coefficients that give an optimal representation of the measurements of the thermal expansion, compressibility, sound speed, and the unreacted shock Hugoniot[9]. It is also noted that the Steinberg-Guinan model for 4340 steel is used for the 4130 steel.

The model gas constituents (HMX D, HMX E, Viton) are treated as no-strength materials with gamma-law equations of state. Note that since the method of slide surfaces was employed, no EOS was needed for the air in the gap. The gamma-law equation of state provides an approximate representation over much of the pressure range, except at the higher pressures of 10 kbar (1 GPa) where the model may be less accurate. The Γ-value for the HE gas species is set using a pressure of 1 kbar (100 MPa), a temperature of 2273^{o}K, and the density and heat capacity from the thermo-chemical equilibrium computer code, CHEETAH 2.0[10] for the final product gases.

The time-dependent thermal transport model includes the effects of conduction, reaction, advection, and compression. The constant-volume heat capacity is constant for each reactant consistent with the Steinberg-Guinan model. The thermal conductivity for the condensed species A and B is taken to be constant, whereas the effects of temperature are included for the gaseous species. The heat capacity for the gases is assigned the same constant-volume value used in the gamma-law model. The temperature-dependent thermal conductivity is estimated at 1 kbar (100 MPa) using Bridgman's equation for liquids[11] in which the sound velocity is calculated using results from CHEETAH.

Parameters for Decomposition Model

The materials parameters for the above decomposition model (Eqns. (1)–(4)) were assembled from measurements obtained for LX-10 samples investigated in earlier studies[12]. Two sets of ODTX measurements were made for LX-10 using the standard apparatus at LLNL (see Figure 7). In this system, the outer surface temperature of a 1.27 cm diameter sphere of HE is suddenly increased to a higher set-point temperature. The time to explosion is the time elapsed from the start of heating until confinement failure. The measurements of this study are plotted as a function of temperature in Figure 7.

Calculated explosion times for LX-10 are also shown in Figure 7 for a one-dimensional model involving transient heat conduction and the chemical reaction sequence (Eqs. (1)-(4) for HMX with inert Viton). The two sets of experimental measurements are well represented by the ALE3D thermochemical model.

It is noted that although this model provides a good representation of ODTX data, it does not adequately represent other types of behavior needed for accurate simulation of thermal transport, time to explosion, and violence in the STEX FCO test of this paper. Two areas of needed model improvement are the areas of pressure effects and the $\beta \rightarrow \delta$ phase transition for HMX.

The decomposition of HMX has been observed to have a strong pressure dependence[13], which is not captured with the present kinetics model. Model decomposition rates are too large when the pressure is small. This decomposition rate strongly influences the STEX vessel pressurization prior to ignition, which would be expected to affect the subsequent violence.

The β→δ phase transition is the second area of needed model improvement. The model β→δ phase transition occurs over many tens of degrees (°C), while past measurements suggest a narrower temperature range. An accurate model for phase transition is important for at least two reasons.

The first reason relates to the 6% decrease in density resulting from the β→δ transition, and its effect on the closing of the gap between the STEX LX-10 charge and the vessel wall. The outside of the STEX LX-10 charge was heated rapidly to temperatures as high as 280°C before ignition while many regions in the interior remained below 100°C (see Figure 3). It is likely that most of the HMX above approximately 160°C transitioned from the β to δ phase. Since there are regions of both β and δ phase HMX through the latter part of the heating phase and ignition phase, the transition dynamics are important for the calculation of the overall expansion of the charge and the closing of the HE-vessel gap.

The β→δ transition also influences the burn behavior of LX-10. The β-phase material burns more slowly (<10X) than the δ-phase material as discussed elsewhere[13]. An accurate phase transition model is needed to predict the regions of β and δ phase in order to satisfactorily represent the STEX burn behavior.

Boundary Conditions and Numerical Method

A one-dimensional, axisymmetric ALE3D model is used to simulate the cookoff of LX-10 in cookoff Test TE-051. The computational domain is the 90° 3D, cylindrical section shown with boundary conditions in Figure 8. This model includes the initial 3% linear gap between the HE and vessel wall. This is the same gap used in the experiment at the axial midplane (see Figure 1). The method of slide surfaces is used to model the air gap, and, thus, no equation of state is employed for the air. However, this model includes thermal conduction and radiation across the air gap. The air thermal conductivity is assigned the value at room temperature and atmospheric pressure. The exchange factor is calculated assuming the emissivities of the steel and HE are 0.25 and 1, respectively.

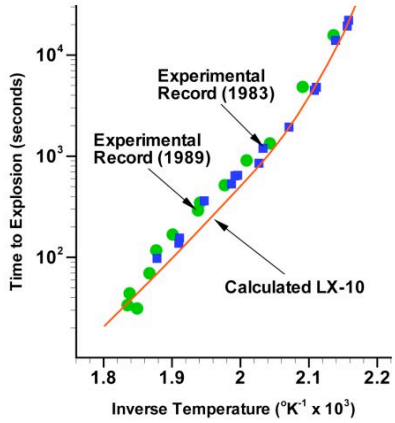

Figure 7. Comparison of model and measured ODTX explosion times as a function of temperature for LX-10.

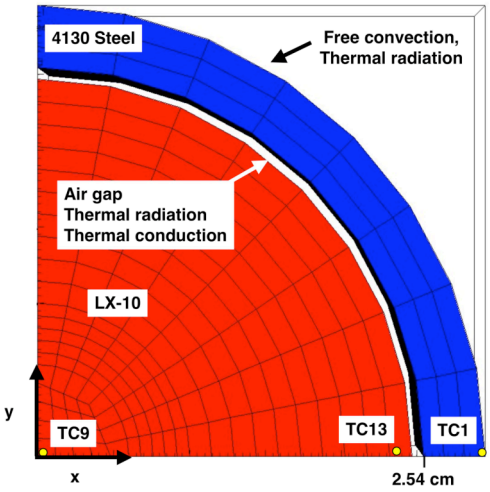

Figure 8. Computational domain, boundary conditions, and mesh for STEX TE-051.

Symmetry conditions are applied at the x=0 and y=0 planes. Slip conditions with no material or energy flow are applied at the z-planes bounding the domain. It is important to note that these z-plane conditions restrict expansion of the materials to the r-direction only. Since the experimental expands in all three directions, the 1D model expansions are approximately 50% higher than the measured values.

The temperature at the outside boundary of the metal cylinder is set at the experimental value for TC1 (see Figure 3). At this time, we decided to focus our attention on the dynamics within the

vessel, and did not perform detailed modeling of the radiant heating used in the experiment. Free convection losses to air at the vessel wall are included using a heat transfer coefficient for laminar flow of air past a vertical plates[14]. A standard expression for hemispherical radiation is used on this same surface.

We used the relatively coarse 3D mesh shown in Figure 8 for the 1D axisymmetric ALE3D model. As decomposition proceeds in the HE solid intermediates and product gases are formed. In elements with more than one species, mixing rules are employed to calculate the energy, temperature, heat capacity, thermal conductivity, shear modulus, and equation of state[15]. The mesh in the HE is smoothed using a combination of Lagrange and Eulerian algorithms. Nodes initially on the HE boundaries remain on these boundaries while nodes interior to the cavity are advected through the HE species. The Lagrangian mesh movement strategy is applied in the steel.

Fully implicit methods are used for the integration of the thermal transport equations and equation of motion during the heating phase. The development of the implicit method for the momentum equation, coupled with chemical reactions, in ALE3D is relatively recent. It replaces the less accurate method of mass scaling used in earlier studies[2, 3]. The improved accuracy is needed for the modeling of dynamic gaps, pressurization prior to ignition, and violence.

This implicit mechanical approach is being developed for use with the method of slide surfaces and gaps employed in this study. It is also being developed for the method of mixed materials in which full materials models are employed for the gap material. The method of slide surfaces is employed in this study since it can accommodate thermal radiation across the gap, which is important in this study. The mixed material approach cannot treat thermal radiation across gaps and is used for slow cookoff cases in which thermal radiation is less important.

After the time step has decreased to within approximately a factor of 10 of the value given by the Courant condition, a switch is made from implicit to explicit integration of the thermal transport and momentum equations. During thermal runaway, the time step often decreases by approximately 14 orders of magnitude to resolve behavior on the dramatically shrinking time scale.

After a temperature reaches a user-specified threshold value, the multi-step kinetics model is replaced by the burn front expression (5). The burn front is propagated through the HE with the assumption that reactants are converted completely to products in a single step. This burn front is tracked using a level set method that conserves mass, momentum, and energy across the front. Since the mesh is not moved to explicitly track the front, the resolution of the burn front is on the scale of the mesh element size. The effects of mesh size are an important consideration under current investigation.

COMPARISON WITH MEASUREMENTS

ALE3D simulations were performed for the STEX fast cookoff experiment (TE-051). The above 1D cookoff model was used with the mesh and boundary conditions of Figure 8. The simulation proceeded to a time of 17.5 minutes (1050 seconds) before terminating. Model temperature fields, temperature traces, strain traces, and gap position variables are shown in Figures 9, 3, 4, and 10, respectively. At early times the temperature difference across the gap is of the scale 100°C, indicating a large resistance to thermal transport. As the temperature increases in the HE, the gap size decreases since the LX-10 CTE of 47×10^{-6} um/m-°C is much larger than the steel value of 12×10^{-6} um/m-°C At t=727 secs (12.1 min), the steel temperature is 284°C, the gap continues to close, and the temperature difference of 122°C C across the gap is decreasing (see Figures 9a and 10). At t=984 sec (16.4 min), the model gap is closed, and the steel hoop strain begins to increase due to the thermal expansion of the HE and generation of HE product gas (see Figure 10). The temperature field at t=1050 secs (17.5 min), shows the gap closed and temperatures ranging from 101°C at the center of the HE to 314°C at the steel case (see Figure 9b).

As mentioned above, the model temperature TC1 at the outside surface of the steel was set to be the measured curve (see Figure 3). The model temperature TC13, at a 1 mm depth in the HE, compares quite favorably with the experimental trace TC12 over the duration of the simulation (see Figure 3). It is noted that although that the surface locations for TC12 and TC13 are different, they are

only 2.5 cm apart and would be expected to have similar temperatures.

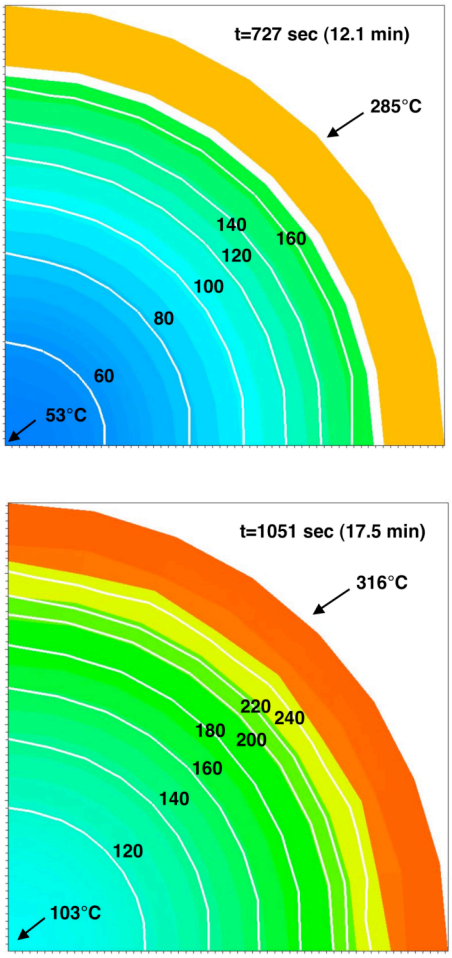

Figure 9. ALE3D model temperature fields for STEX fast cookoff test TE-051.

The agreement between model and measured temperature profiles suggests that the model captures important thermo-mechanical behavior for the gap closing. However, there is a sharp upward bend in the model curve for TC13 at 16.2 min when the model gap is closing. This feature is not seen in the experimental curve. The model curve for TC9 at the center of the HE is similar to the experimental curve at early times, but increases more rapidly than the measured curve at later times. The model does not include the axial flow of heat towards the vessel end caps, which would provide cooling for the interior HE.

The model hoop strain, scaled by a factor of 2/3, is compared with the measured hoop strain at SG2 in Figure 4. The factor of 2/3 is included to compensate for the absence of axial expansion in the model system, which is present in the physical system. The 2/3Xmodel and measured hoop strain curves are similar until t=16.4 min, the time at which the model gap closes. Before this time, the differences between the measured value for SG2 and the model hoop strain can in part be attributed to the lower temperature (TC4) at SG2 versus the higher temperature of TC1 used in the model.

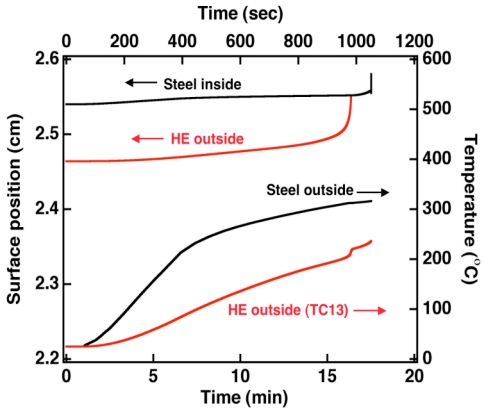

Figure 10. ALE3D model gap position variables for STEX test TE-051 with LX-10 confined in a 4130 steel vessel.

After the gap closure at t=16.4 min, the model hoop strain in the solid increases more rapidly due to the thermal expansion of the solid HE and the generation of product gas. In contrast, the measured strain curves of Figures 4 and 6 indicate that the solid HE did not come into contact with the HE until the ignition phase, approximately 400 microseconds prior to the trigger of the break wire.

An important contribution to the early closure of the model gap is the 1.5X larger values for the model expansions in the radial direction resulting from the motion constraints in the axial direction, as discussed above. This difficulty can be remedied by employing 2D and 3D models incorporating the axial direction.

A second effect contributing to the early closure of the model gap is the treatment of gas flow. The model HE decomposition gases are mixed with the solid constituents, and cannot flow preferentially through the porous solid HE to the gap region as they would in the physical system. As the decomposition gases are generated, the

model solid-liquid mixture expands until it makes contact with the vessel wall. In effect the solid HE is being artificially carried with the expanding gas towards the vessel wall closing the gap. A model for product gas flow in porous HE is being added to ALE3D to improve this situation.

The third effect that would likely contribute to the early gap closure is the absence of a pressure-dependence for the present chemical kinetics model. At the low pressures occurring during the early stages of decomposition, the present kinetics model generates gas at a rate much larger than is measured. This behavior would also lead to early closure of the gap.

CONCLUSIONS

An experimental and numerical investigation was performed to characterize heat transfer and violence for the fast cookoff of LX-10 confined in a 4130 steel vessel. The thermal measurements showed temperature differences larger than 100°C across HE-vessel gap. This benchmark STEX experiment included several diagnostic systems to measure violence at various stages of the thermal explosion. Measurements from a strain gauge, three PDV probes, and micropower radar units were combined to determine wall position versus time for 15 cm of motion. A fragment size distribution constructed for the recovered fragments gave a median fragment mass of 1.1 g. The explosion was a violent deflagration based on the mean radar velocity of 840 m/s, the 80 μs time scale of the explosion, and the measured fragment sizes.

We performed ALE3D 1D axisymmetric simulations for this fast cookoff test. A four-step Tarver-McGuire model was used to represent the chemical kinetics. The 1D model included thermal expansion and thermal transport by conduction and radiation across a closing gap. Unfortunately, numerical difficulties halted this simulation just prior to ignition. However, the ALE3D model provided a good representation of the temperature rise at the HE surface and the interior HE at early times. This suggests that the model captured the important features of heat transfer across the dynamic gap between the steel case and the explosive. This is a key step to predicting the ignition time and the violence of explosion.

ACKNOWLEDGMENTS

We are grateful for the many contributions to this project. Rich Becker and Jim Reus developed the new implicit routines for slow mechanics in ALE3D. Greg Sykora set up the STEX control and diagnostic system. Kevin Black helped with the buildup of the STEX apparatus. Carlos Romero and Kique Romero set up and operated the PDV and radar systems, respectively.

REFERENCES

1. Maienschein, J. L. and J. F. Wardell, "The Scaled Thermal Explosion Experiment," Proceedings of 12th International Detonation Symposium, San Diego, CA, 2002.

2. Yoh, J. J., M. A. McClelland, J. L. Maienschein, J. F. Wardell and C. M. Tarver, "Simulating thermal explosion of cyclotrimethylenetrinitramine-based explosives: Model comparison with experiment," *J. Appl. Phys.*, vol. 97, pp. 083504-1-11, 2005.

3. Yoh, J. J., M. A. McClelland, J. L. Maienschein, A. L. Nichols and C. M. Tarver, "Simulating thermal explosion of octahydrotetranitrotetrazine-based explosives: Model comparison with experiment," *J. Appl. Phys.*, vol. submitted, pp. 2006.

4. McClelland, M. A., J. L. Maienschein, J. E. Reaugh, T. D. Tran, A. L. Nichols and J. F. Wardell, "ALE3D Model Predictions and Experimental Analysis of the Cookoff Response of Comp B," Proceedings of JANNAF 39th Combustion and 21st Propulsion Systems Hazards Subcommittee Meetings, Colorado Springs, CO, 2003.

5. McClelland, M. A., J. L. Maienschein, J. J. Yoh, M. R. deHaven and O. T. Strand, "Measurements and ALE3D Simulations for Violence in a Scaled Thermal Explosion Experiment with LX-10 and AerMet 100 Steel," Proceedings of JANNAF 40th Combustion and 22st Propulsion Systems Hazards Subcommittee Meetings, Charleston, SC, 2005.

6. Knap, J., M. A. McClelland, J. L. Maienschein, W. M. Howard, A. L. Nichols, M. R. deHaven and O. T. Strand, "MEASUREMENT AND ALE3D SIMULATION OF VIOLENCE IN A DEFLAGRATION EXPERIMENT WITH LX-10 AND AERMET-100 ALLOY," Proceedings of 13th International Detonation Symposium, Norfolk, VA, 2006.

7. McClelland, M. A., J. L. Maienschein and A. L. Nichols, "Joint DoD/DOE Munitions Technology Development Program FY-01 Progress Report, Ignition

and Initiation Phenomena: Cookoff Violence Prediction," Lawrence Livermore National Laboratory, 2002.

8. Tarver, C. M. and T. D. Tran, " Thermal decomposition models for HMX-based plastic bonded explosives " *Combustion and Flame*, vol. 137, pp. 50-62, 2004.

9. McClelland, M. A., T. D. Tran, B. J. Cunningham, R. K. Weese and J. L. Maienschein, "Cookoff Response of PBXN-109: Material Characterization and ALE3D Thermal Predictions," Proceedings of 50th JANNAF Propulsion Meeting, Salt Lake City, UT, CPIA, 2001.

10. Fried, L. E., W. M. Howard and P. C. Souers, "Cheetah 2.0 User's Manual," Lawrence Livermore National Laboratories, UCRL-MA-117541 Rev. 5, 1998.

11. Bird, R. B., W. E. Stewart and E. N. Lightfoot, *Transport Phenomena,* Wiley, pp. 260-261, 1960.

12. Tran, T. D., "A Complilation of One-Dimensional, Time-to-Explosion (ODTX) Data for High Explosives and Propellants," Lawrence Livermore National Laboratory, UCRL-ID-151449, 2003.

13. Hsu, P. C., "Characterization of Damaged Materials," Proceedings of 13th International Detonation Symposium, Norfolk, VA, 2006.

14. Holman, J. P., *Heat Transfer,* McGraw-Hill, pp. 253-254, 1976.

15. Sharp, R., "Users Manual for ALE3D An Arbritrary Lagrange/Eulerian 3D Code System," Lawrence Livermore National Laboratory, 2005.